ATOMISTIC SIMULATIONS OF TWIN BOUNDARIES FACETING IN HCP MATERIALS

OSTAPOVETS Andriy

Institute of Physics of Materials (CEITEC-IPM), Academy of Sciences of the Czech Republic, Brno, Czech Republic EU, ostapov@ipm.cz

Abstract

Deformation twinning is frequently observed in materials with hexagonal crystal lattice. It plays important role in plastic deformation of such materials. Twin regions have often lamellar shape and twin boundaries are usually oriented along invariant planes. However, non-invariant plane twin interfaces are also observed. Occurrence of such interfaces can be connected with interactions between twinning disconnections. Mechanisms of such interactions are discussed on the basis of atomistic simulations.

Keywords: Twin boundaries, hcp, EAM potential, faceting, disconnection

1. INTRODUCTION

Deformation twinning plays significant role in plastic deformation of hcp materials [1]. The twinning deformation is represented by shear, which takes place along the plane traditionally designated as K1 in the twinning direction η1. Twinning mode is usually characterized by a set of four twinning elements K1, η1, K2, η2, where K2, η2 are the second undistorted, but rotated, plane and direction respectively. Twin regions have often lamellar shape and twin boundaries are usually oriented along invariant planes. These invariant planes are undistorted under twinning shear. However, twin boundaries significantly inclined from K1 planes are also observed [2]. These boundaries may be called non-invariant plane twin interfaces. For instance, basal-prismatic twin boundary associated with $\{10\bar{1}2\}$ twins was observed in magnesium [3], cobalt [2] and titanium [4].

Development of twin boundary faceting can be caused by interactions between twinning disconnections [5]. The disconnections are defects responsible for twin boundary migration [5, 6]. They are linear dislocation-like defects, which similar to dislocations can be characterized by Burgers vector. However, disconnections also produce step on the twin boundary in contrast to dislocations.

In our previous papers [3, 5, 7] we shown, that basal-prismatic facets in $\{10\bar{1}2\}$ twin boundary in magnesium are results of interactions between b2/2 disconnections. The aim of present paper is discussion of possible $\{10\bar{1}1\}$ twin boundary faceting developed in the similar way, i.e. by interaction of twinning disconnections. Faceting of $\{10\bar{1}1\}$ boundary was observed experimentally [8], where presence of $\{10\bar{1}0\}$ / $\{10\bar{1}3\}$ facets was reported. Several twinning modes are observed on $\{10\bar{1}1\}$ plane in contrast to twinning on $\{10\bar{1}2\}$ plane. These modes have the same twinning plane K1, but different twinning directions η1. Each of the twinning modes can be associated with motion of corresponding disconnection. The disconnection with step height equal to two interplanar distances (b2/2) has the highest mobility [9]. However, the disconnection with four interplanar distances step height (b4/4) leads to twinning parameters, which are the closest to experimentally observed parameters of deformation twins. It was proposed in [10] that correct twinning direction for $\{10\bar{1}1\}$ deformation twin can be produced by motion of equal numbers of b2/2 disconnections with alternating signs of screw dislocation component.

Model of interactions between b2/2 disconnections is considered in the present paper. The modelling is performed for $\{10\bar{1}1\}$ twin in generic hcp material with c/a = 1.5. Such material represents a degenerated case with Burgers vector of b4/4 disconnection is equal to 0. Consequently, only the b2/2 disconnections can be considered.

2. METHODS

Atomistic simulations were performed in LAMMPS [11] with generic EAM potential. The potential (1) is taken in a simple analytical form with only five parameters *A*, *ξ*, *p*, *q*, r_0 proposed by Rosato and co-workers [12].

$$U = -\sum_i (E_b^i + E_r^i)$$
$$E_b^i = -\left\{\sum_j \xi^2 exp\left[-2q\left(\frac{r_{ij}}{r_0}-1\right)\right]\right\}^{1/2} \quad (1)$$
$$E_r^i = \sum_j A exp\left[-p\left(\frac{r_{ij}}{r_0}-1\right)\right]$$

The version of potential used in the current paper was designated as p9q1.5 in the [13]. The potential was fitted according to procedure described in [13]. The parameters *p* and *q* were varied freely to change potential properties. Fitting was performed to cohesive energy (-2.95 eV) and lattice parameter (0.409 nm) of fcc silver. The fifth parameter r_0 is equal to the first neighbour separation. Both the bonding, E_b^i, and repulsive, E_r^i, energy contributions for an *i*-atom are cut at the distance corresponding to the 3th neighbours of fcc lattice. Between the 3rd and 4th neighbours, the exponential expressions for E_b^i and E_r^i are replaced by fifth order polynomials. The polynomial coefficients are fitted to obtain continuity of the values and first and second derivatives at the point of line-up (the 3rd neighbour separation) and truncation to zero at the cut-off distance. The potential does not describe any specific material. The fitting was performed only in order to obtain reasonable scaling. The parameters of p9q1.5 potential are listed in **Table 1** together with parameters of model material. This potential stabilizes hcp structure with *c*/*a* = 1.5.

Table 1 Parameters of p9q1.5 potential and model material

Potential parameter, *p*	9
Potential parameter, *q*	1.5
Potential parameter, *A*	0.058
Potential parameter, *ξ*	0.902
Potential parameter, r_0	2.892
Potential cut-off	0.5784 nm
Lattice parameter, *a*	0.2920 nm
c/*a* ratio	1.5
Cohesive energy, *E*	-2.96 eV

Simulation block was oriented with *x* axis along $\langle 10\bar{1}2\rangle$; *y* axis along normal to $\{10\bar{1}1\}$ plane and *z* axis along $\langle 2\bar{1}\bar{1}0\rangle$ direction. The disconnections with step height equal to two $\{10\bar{1}1\}$ interplanar distances and Burgers vector $\boldsymbol{b}_{2/2} = 1/6\langle 2\bar{1}\bar{1}0\rangle$ were inserted into the block containing perfect twin boundary by imposing of corresponding elastic displacement field. In general, the Burgers vector direction is dependent on the lattice parameters defined by the interatomic potential. However, due to special *c*/*a* ratio (equal to 1.5), the Burgers

vector of the twinning dislocation is aligned with <*a*> direction in our simulations. Dislocation line was oriented along z direction in our simulation.
The modeling was performed in the following steps. Set of disconnections was inserted into the block. Then shear deformation was applied to the block in small increments and energy minimization by conjugate gradient method was performed. The periodical boundary conditions were applied in *z*-direction; block had free surfaces in *x*-direction and fixed boundary conditions were applied in *y*-direction i.e. positions of several atomic layers near the surface were fixed during simulations.

3. RESULTS AND DISCUSSION

Structure of considered $\boldsymbol{b}_{2/2}$ disconnection is presented in **Fig. 1**. The disconnection produces step on the $\{10\bar{1}1\}$ boundary. The step edges are parallel to (0001) plane in one of the grains and to $\{10\bar{1}1\}$ in other one. The structures of twin boundary and the twinning disconnection are similar to those observed in titanium [6]. However the $\boldsymbol{b}_{2/2}$ disconnection aligned along $[1\bar{2}10]$ direction exhibits pure screw character in our case in contrast to the mixed disconnection in [6]

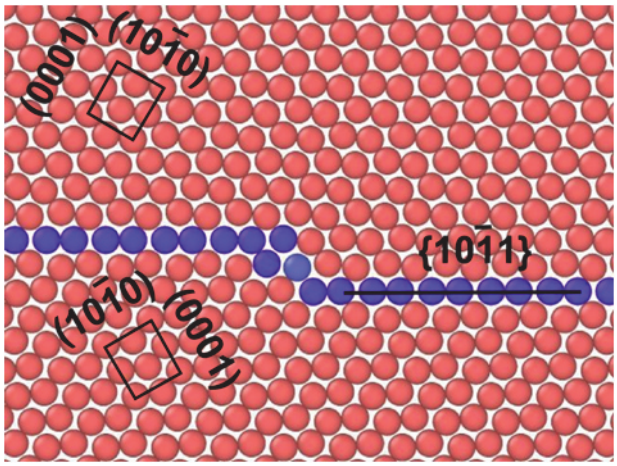

Fig. 1 Disconnection in $\{10\bar{1}1\}$ twin boundary. Projection in $[1\bar{2}10]$ direction. Hcp lattice cells are marked by rectangles in both sides of the boundary. Blue atoms have surroundings different from the bulk

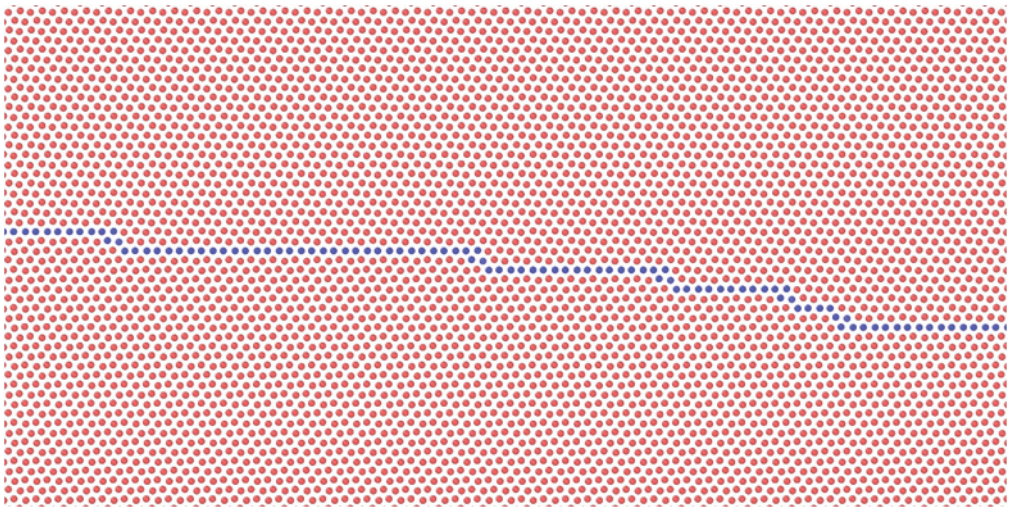

Fig. 2 Initial configuration of twin boundary containing five disconnections

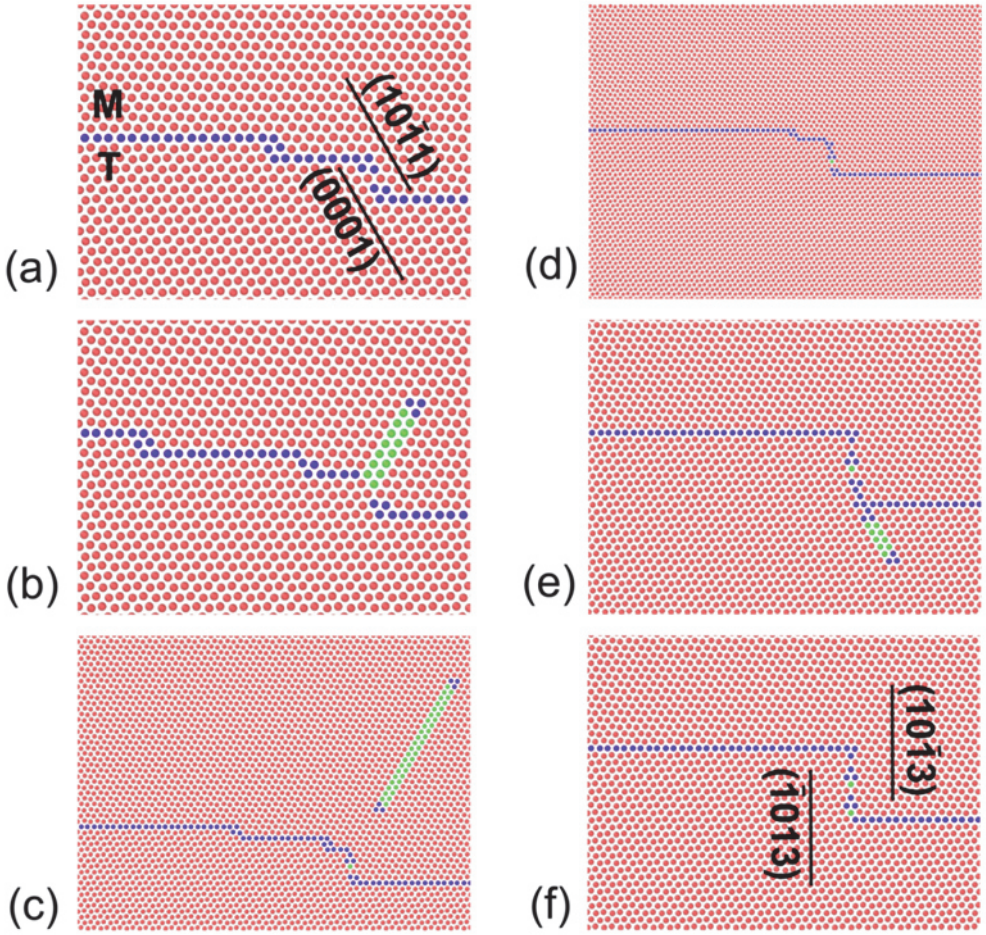

Fig. 3 Evolution of disconnection structure and facet development under applied shear strain: (a) formation of $(0001)/\{10\bar{1}1\}$ facet by interaction of two twinning disconnections; (b) emission of basal stacking fault from facet; (c) transformation of stacking fault into spread core of basal dislocation; (d) interaction with further disconnections; (e) emission of second basal dislocation; (f) development of $(\bar{1}013)/\{10\bar{1}3\}$ facet

Fig. 2 shows the initial configuration of twin boundary with five imposed disconnections. An obstacle for disconnection movement was inserted into the boundary after initial energy relaxation. The obstacle was made by zeroing atomic forces in several atomic layers lying to right side from the leading disconnection. In order to study disconnection motion, the $\{10\bar{1}1\}[1\bar{2}10]$ shear deformation was applied to the block. Evolution of disconnection structure under applied deformation is presented in **Fig. 3**. In very beginning, the first disconnection is stopped by obstacle. The next disconnection reaches the leading one and together they produce $(0001)/\{10\bar{1}1\}$ facet (**Fig. 3a**). Previous studies [3, 5, 7] show that "pile-up" of several disconnections in $\{10\bar{1}2\}$ twin boundary leads to formation of relatively long basal-prismatic facets. However, $(0001)/\{10\bar{1}1\}$ facets do not grow by joining the next disconnection in the present case. Such behaviour can be explained by the fact that Burgers vector length of considered disconnections is higher than Burgers vector length of $\{10\bar{1}2\}$ twinning disconnections. Consequently, repulsive forces between disconnections are higher. Basal stacking fault is emitted from the facet with further increase of loading (**Fig. 3b**). The fault is limited by partial dislocation with Burgers vector $\boldsymbol{b}_p = 1/3[\bar{1}100]$. Then this stacking fault is transformed to spread core of basal slip dislocation $\boldsymbol{b} = 1/3[\bar{1}2\bar{1}0]$ (**Fig. 3c**) by nucleation of another partial with $\boldsymbol{b}_p = 1/3[01\bar{1}0]$. The emission of basal slip dislocation leads to change of Burgers vector sign of one of disconnection. Consequently, the facet

becomes to contain the set of disconnections with alternating signs. Further decrease of facet energy is reached by aligning of disconnections to produce $(\bar{1}013)/\{10\bar{1}3\}$ facet (**Fig. 3d**). This facet also emits basal slip dislocation after subsequent joining of disconnections gliding along $\{10\bar{1}1\}$ twin boundary (**Fig. 3e**). The joining of five disconnections leads to formation of $(\bar{1}013)/\{10\bar{1}3\}$ shown in **Fig. 3f**. It is worth to note that $(\bar{1}013)/\{10\bar{1}3\}$ boundary is the twin boundary for conjugate twin mode. Consequently, the formation of such facet is similar to formation of conjugate $\{10\bar{1}2\}$ facets in $\{10\bar{1}2\}$ boundaries reported previously [6, 7].

4. CONCLUSION

Interactions of $\boldsymbol{b}_{2/2}$ twinning disconnections in $\{10\bar{1}1\}$ twin boundary can lead to formation of $(0001)/\{10\bar{1}1\}$ and $(\bar{1}013)/\{10\bar{1}3\}$ facets. The length of obtained facets is relatively small in contrast to length of basal-prismatic facets observed in $\{10\bar{1}2\}$ twin boundaries. The facets can optimize their structure by emission of bulk dislocations.

ACKNOWLEDGEMENTS

Author acknowledges support from the Ministry of Education, Youth and Sports of the Czech Republic (grant number CZ.1.07/2.3.00/30.0063); Academy of Sciences of the Czech Republic, project no. RVO: 68081723; the Central European Institute of Technology (CEITEC) with research infrastructure supported by project CZ.1.05/1.1.00/02.0068.

REFERENCES

[1] CHRISTIAN J.W., MAHAJAN S. Deformation twinning. Progress in Materials Science, Vol. 39, 1995, 157 p.

[2] ZHANG X.Y., LI B., WU X., ZHU Y.T., MA Q., LIU Q., WANG P.T., HORSTEMEYER M.F. Twin boundaries showing very large deviations from the twinning plane. Scripta Materalia, Vol. 67, 2012, pp. 862-865.

[3] OSTAPOVETS A., MOLNÁR P., GRÖGER, R. On basal-prismatic twinning interfaces in magnesium. IOP conference series: Materials Science and Engineering, Vol. 63, 2014, p. 012134.

[4] SUN Q., ZHANG X.Y., TU J., REN Y, QIN, H., LIU Q.C. Characterization of basal-prismatic interface of {1012} twin in deformed titanium by high-resolution transmission electron microscopy. Philosophical Magazine Letters, Vol. 95, No. 3, 2015, pp. 145-151.

[5] OSTAPOVETS A., GRÖGER, R. Twinning disconnections and basal-prismatic twin boundary in magnesium. Modelling and Simulations in Materials Science and Engineering, Vol. 22, 2014, pp. 509-516.

[6] POND R.C., BACON D.J., SERRA, A. Interfacial structure of {1011} twins and twinning dislocations in titanium. Philosophical Magazine Letters, Vol. 75, No. 5, 1995, pp. 275-284.

[7] OSTAPOVETS A., SERRA A. Characterization of the matrix-twin interface of {1012} twin during growth. Philosophical Magazine, Vol. 94, No. 25, 2014, pp. 2897-2839.

[8] LI Y.J., CHEN Y.J., WALMSLEY J.C., MATHINSEN R.H., DUMOULIN S., ROVEN H.J. Faceted interfacial structure of {1011} twins in Ti formed during equal channel angular pressing. Scripta Materialia, Vol. 62, 2010, pp. 443-446.

[9] SERRA A., POND R.C., BACON D.J. Computer simulation of the structure and mobility of twinning dislocations in H.C.P. metals. Acta Metallurgica et Materialia, Vol. 39, 1991, pp. 1469-1480.

[10] WANG J., BEYERLEIN I.J., HIRTH J.P., TOME C.N. Twinning dislocations on {1011} and {1013} plane in hexagonal close-packed crystals. Acta Materialia, Vol. 59, 2011, pp. 3990-4001.

[11] PLIMPTON S. Fast parallel algorithms for short-range molecular dynamics. Journal of Computational Physics, Vol. 117, 1995, pp. 1-19.

[12] ROSATO, V., GUILLOPE, M., LEGRAND, B. Thermodynamical and structural properties of f.c.c. transition metals using a simple tight-binding model. Philosophical Magazine A, 59, 1989, pp.321-336.

[13] OSTAPOVETS A., PAIDAR V. Properties of exponential many-body interatomic potentials, Kovove Materialy, Vol. 47, 2009, pp. 193-199.